Optica Applicata, Vol. XXXII, No. 3, 2002

Optimized structure of SiC_xN_y–Si(111) interfaces by molecular dynamics simulation

WOJCIECH GRUHN, IVAN V. KITYK

Institute of Physics, Pedagogical University, al. Armii Krajowej 13/15, 42–201 Częstochowa, Poland.

The SiC_xN_y films were synthesized using a technique of chemical evaporation at low pressures. Films with thickness varying between 8 and 24 nm and with an N/C ratio between 0.1 and 1.5 were obtained. The stoichiometry of these films was measured after their deposition on Si(111) substrates using an extended X-ray absorption fine structure (EXAFS) method. Distances between C–Si and C–N atoms, as well as the molecular dynamics simulations, were done. A comparison of the experimentally obtained and molecular dynamics optimized geometry structure is done. Exchange-correlation potential within a framework of the local density functional approach gives the similar C–Si and C–N bond distances as with inclusions of the non-local many-body screening potential. At the same time pressure derivatives within the local density approach agree better with experimental data.

1. Introduction

Due to their technological importance, silicon oxynitrides have been the subject of increasing research interest in recent years [1]. Among the nitrides, the SiC_xN_y films may be more interesting for the optoelectronics because they are more technological. The major problem, which must to be resolved, consists in determining parameters of the electron structure with respect to the nitrogen/carbon (N/C) content. The traditional structure methods [1] are not sufficient in this case. We compare theoretical approaches within a framework of local density approach (LDA) with experimentally obtained structural data. The sensitivity of the proposed theoretical molecular dynamics method both to the N/C ratio, as well as to the film thickness, is discussed [2], [3]. Several discrepancies between the experimentally obtained and theoretically calculated distances between the C–Si and C–N bonds are analyzed.

2. Experimental technique

The films were deposited by thermal low pressure chemical vapor deposition on Si(111) substrate (described, for example, in paper [2]). The entire process was performed using an ultra-high vacuum cold wall chamber with a pressure of about 4×10^{-8} mbar. The Si(111) substrate was heated by radiation from a tungsten lamp.

Such equipment enables us to accelerate the evaporation process. High-purity gases (SiN_2Cl_2, NH_3 and CN), the contents of which were controlled with precision up to 0.2%, were used as a source in this process. The N/C ratio was changed by continuous variation of the CN/NH_3 ratio. The growth rate, which was dependent on the N/C ratio, was selected using the Habraken rule [3]. The temperatures of the specimens were varied within the range 300–1201 K. This equipment allowed us to achieve thermostabilization with precision up to 0.1 K. The film thickness was varied by the deposition time. The homogeneity and stoichiometry of the films were measured using Auger electron spectroscopy. The thickness and the refractive index of each film were independently determined by ellipsometry using a variable angle spectroscopic ellipsometer from Woolan Co. All the structural-content control measurements were carried out after deposition of the film. The EXAFS method was used to pick out SiC_xN_y specimens with the desired N/C ratio and thickness.

During the molecular dynamics simulations we have used a special approach developed for chalcogenide glasses and large-sized SiC nanocrystallites [4]. In paper [5] the procedure of the molecular dynamics calculations has been described using the Hartree–Fock non-local many-body screening potential. In this paper we have replaced the non-local many-body interactions by the Pedrew–Alder exchange-correlation potential [6]. This potential is parametrized within the local density functional (LDF) approach and may be considered as an effective tool for reconstructing crystalline states near the interfaces.

The main steps of our approach are as follows: appropriate molecular dynamics geometry optimization and seeking a minimum of the total energy; *ab initio* calculations of the electronic structure in the vicinity of the interfaces; taking into account the electron-phonon interaction including anharmonic interactions; contribution of the interface mesoscopic interactions.

Geometry optimization was carried out in order to determine the electron density of states (DOS), the main cation-anion tetrahedral bonds, and particularly the C–Si and C–N distances.

3. Theoretical approach and results

The structure is considered to be a superposition of the Si(111) single crystal long-range ordered fragments disturbed by amorphous-like SiC_xN_y films. The structure of the interface region was built using the molecular dynamics simulations developed for large-sized nanocrystallites described in detail by the authors in the paper [7]. The region near the interfaces between the and the films was built using a successive "step-by-step" procedure described in [7]. In this approach the films are considered to be nanocrystallites with sizes fined by the structural TEM data (see the Table).

Necessary quasi-Brillouin zone integration was achieved using a linear tetrahedral method with a grid of 896 **k**-points in the irreducible part of the quasi-Brillouin zone. The cluster sizes were evaluated from structural data obtained from the TEM experiments.

T a b l e. TEM measured averaged sizes of the SiC_xN_y grains *vs.* the N/C ratio and film thickness *d*.

d [nm]	N/C = 0.3	N/C = 0.6	N/C = 0.9	N/C = 1.2	N/C = 1.5
8	2.03±0.15	2.06±0.15	2.11±0.15	2.15±0.15	2.18±0.15
12	1.97±0.15	2.07±0.15	2.10±0.15	2.17±0.15	2.21±0.15
16	2.07±0.15	2.11±0.15	2.18±0.15	2.26±0.15	2.23±0.15
20	2.11±0.15	2.14±0.15	2.21±0.15	2.25±0.15	2.22±0.15
24	2.18±0.15	2.14±0.15	2.23±0.15	2.25±0.15	2.22±0.15

The equilibrium atom positions were obtained from the condition for the minimum of the total energy as a function of the electron charge density $\rho(r)$. As a starting point we applied the hybrid Becke's method [8] within the density functional theory (DFT) approach, together with the gradient-corrected correlation functional E_C^{LSDA}. The DFT calculations were performed using the GAUSSIAN 94 program and the Perdew–Alder exchange-correlation screening potential [5]. The main advantage of this method is a very fast convergence of eigenvalues with respect to the sizes of the basic sets.

The initial wave functions were taken for ideal Si crystals. Then we replaced the Si atoms successively by N and C appropriate ratios and carried out the geometry optimization by iterations. During this procedure the tetrahedral Si crystalline structure was substantially deformed, and the tetrahedra were transformed into hexagons.

The quantum chemistry calculations were carried out self-consistently after the separation of the electron and phonon degrees of freedom. The Schrödinger equation for a pure phonon motion was expressed in a harmonic approximation

$$\frac{\mathrm{d}^2\Psi_k}{\mathrm{d}Q_k^2} + (-4\pi^2\mu_k h^{-2}Q_k^2 + 8\pi^2\mu_k h^{-2}\Omega_k)\Psi_k = 0 \tag{1}$$

where Ψ_k is a wave function corresponding to k-th normal coordinate Q_k; μ_k denotes a reduced mass of the nuclei taking part in the k-th phonon mode. It is clear that solutions of the above equation are determined by a model that is responsible for the force constant calculations (the so-called Hessian matrices). The eigenenergy of the k-th phonon's mode is expressed as

$$\Omega_k(v_k) = 2\Omega_{k0}\left(v_k + \frac{1}{2}\right) \tag{2}$$

where Ω_{k0} is a zero-point motion energy, and $v_k = 0, 1, 2, \ldots$ is the phonon quantum number associated with the following wave function:

$$\Psi_k(Q_k) = \left(\frac{2\Omega_{k0}}{\pi}\right)^{1/2}(2^{v_k}v_k!)^{-1/2}\exp(-\Omega_{k0}Q_k^2)H_v[(2\Omega_{k0})^{1/2}Q_k] \tag{3}$$

where $H_v(x)$ is a Hermite polynomial of v-th order. The application of Eq. (2) is

physically justified by the localization of the mesoscopic clusters. Changes in the clusters, in accordance with this equation, may be described as a local perturbation.

To introduce the electron–phonon interaction, the electron–phonon potential $V_{\text{e-ph}}(\mathbf{r}_i)$ was calculated in a nonlinear approximation [8]

$$V_{\text{e-ph}}(\mathbf{r}_i) = e^2 \sum_{ms} M_{ms}^{-1/2} \left[Z_{ms}(\mathbf{r}_s - \mathbf{u}_{ms}) |\mathbf{r}_s - \mathbf{u}_{ms}|^{-3} - \sum_{m's'} Z_{m's'}(\mathbf{r}_{s'} - \mathbf{u}_{m's'}) |\mathbf{r}_{s'} - \mathbf{u}_{m's'}|^{-3} \right] \tag{4}$$

where M_{ms} and Z_{ms} are effective ionic mass and charge with corresponding ions numbered by m and s, respectively. The $\mathbf{u}_{ms}$ vector is a relative displacement of two interacting ions from their equilibrium positions $\mathbf{r}_s$ and $\mathbf{r}_{s'}$. Probability of a one-phonon transfer induced by the phonon of a frequency Ω_k is equal to

$$W^-(\Omega_k) = 4\left(\frac{h}{2\pi}\right)^{-2} c^{-3} H^{-1} g^{-1}(\mathbf{r}_i)(\mathbf{E}_{el} - \Omega_k)^2 B^-(\Omega_k) \tag{5}$$

where H is a sum of the η and ξ levels widths; E_{el} denotes energy of the inter-band transitions; Ω_k denotes a k-th phonon energy and $g(\mathbf{r}_i)$ is a degeneration degree of corresponding electron energy levels. The parameter $B^-(\Omega_k)$ (determining the photoinduced changes) is expressed by [9]

$$B^-(\Omega_k) = \sum_{\eta}^{g(\eta)} \sum_{\xi}^{g(\xi)} \left| \sum_{\varphi} \langle \eta, \eta_\Omega | V_{\text{e-ph}}(\mathbf{r}_i) | \xi, \eta_{\Omega+1} \rangle \langle \varphi | \mathbf{d} | \xi \rangle (E_\xi - E_\eta + \Omega_k)^{-1} + \sum_{\varphi} \langle \varphi | \mathbf{d} | \xi \rangle \langle \eta, \eta_\Omega | V_{\text{e-ph}}(\mathbf{r}_i) | \xi, \eta_{\Omega-1} \rangle (E_\xi - E_\eta + \Omega_k)^{-1} \right|^2 \bar{\theta} \tag{6}$$

where φ denotes a virtual intermediate molecular orbital (MO) electron state, $\mathbf{d}$ is an electric dipole moment for a given optical transition; η_Ω and η, ξ correspond to the electronic and phonon states, respectively. The sums are performed over all degenerate initial and final states. $\bar{\theta}$ is the average of the occupation numbers of the electron-phonon states with frequency Ω_k. We found that an increase in the nitrogen content favoured the appearance of hexagonal-like structural fragments. An excited quasi-phonon contribution was then included, using the method described in paper [10].

The symmetric phonons included in the electron-phonon interaction (Eqs. (4)–(6)) lead to the following normal coordinates:

$$B^-(\Omega_k) = C_\eta \xi^\gamma(r_\lambda^\Delta) C_{\eta'} \xi^{\gamma'}(r_{\lambda'}^{\Delta'}) \operatorname{Im} G_{\Delta\Delta'}^{\gamma\gamma'}(r_\lambda^\Delta, \Omega_k^2) \tag{7}$$

where $G^{\gamma\gamma'}_{\Delta\Delta'}$ is a Green function (γ and γ' are numbers of coordination sphere) defined as

$$G^{\gamma\gamma'}_{\Delta\Delta'}(r^{\Delta}_{\lambda}) = \sum_{\varphi} [\langle \eta | V_{\text{e-ph}}(\mathbf{r}_i) | \varphi \rangle \langle \varphi | \mathbf{d} | \xi \rangle + \langle \eta | \mathbf{d} | \varphi \rangle \langle \varphi | V_{\text{e-ph}}(\mathbf{r}_i) | \xi \rangle] (E_{\xi} - E_{\eta k})^{-1}. \tag{8}$$

The resulting expression is given below

$$G^{\gamma\gamma'}_{\Delta\Delta'}(r^{\Delta}_{\lambda}, \Omega^2_k) = \sum_{\Omega} K^{\gamma'}_{\Delta'}(r^{\Delta'}_{\lambda'}) K^{\gamma}_{\Delta}(r^{\Delta}_{\lambda}) (\Omega^2_k - \Omega^2 - i\delta)^{-1} \tag{9}$$

where the generalized coordinates $K^{\gamma}_{\Delta}(r^{\Delta}_{\lambda})$ are obtained for a given phonon type from the averaged electron states. Taking into account cluster deformation localization, we have applied the Dyson expressions [5], [6], [8]. The deformation potential (due to superposition of the different clusters) and corresponding interface charge density disturbance determine the potential operator U

$$G^{\gamma\gamma'}_{\Delta\Delta'}(1) = G^{\gamma\gamma'}_{\Delta\Delta'}(0) + G^{\gamma\gamma'}_{\Delta\Delta'}(0) U G^{\gamma\gamma'}_{\Delta\Delta'}(1) \tag{10}$$

where $G^{\gamma\gamma'}_{\Delta\Delta'}(0)$ is a Green function for the harmonic subsystems, and $G^{\gamma\gamma'}_{\Delta\Delta'}(1)$ is a Green function for subsystems disturbed by the anharmonic electron-phonon potential U.

4. Results of simulations – comparison with experiments

Figures 1 and 2 present the results of the molecular dynamics simulations of the C–Si and C–N bond lengths with respect to the N/C ratio and film thickness d, carried out using the method described above. It can be seen that increase in the film thickness leads to the increase in the C–Si distance from 1.89 Å to 1.91 Å. For the N/C ratio of approximately 0.5, the C–Si distance achieves its maximum at a thickness of about 1.892 Å. A further increase in the N/C ratio leads to a shift of the observed maximum positions towards the lower thickness (up to 12.5 nm for the N/C ratio of about 1.5). The existence of maxima reflects a kind of "competition" between long-range ordering due to the Si crystalline surface and randomly amorphous-like disordering due to the introduction of the N and C in the Si positions. Carbon and nitrogen cause opposite changes in the charge density distribution, and therefore in the interface electrostatic potential distribution near the SiC_xN_y–Si(111) interface. It is worth emphasizing that there is a good agreement between the structural data obtained using the non-local correlation functions [5] and the Perdew–Alder exchange-correlation screening potential [6].

The thickness dependence of the C–N distances is substantially different. At first glance, one can see in (Fig. 2) several content-thickness maxima: the first one is at

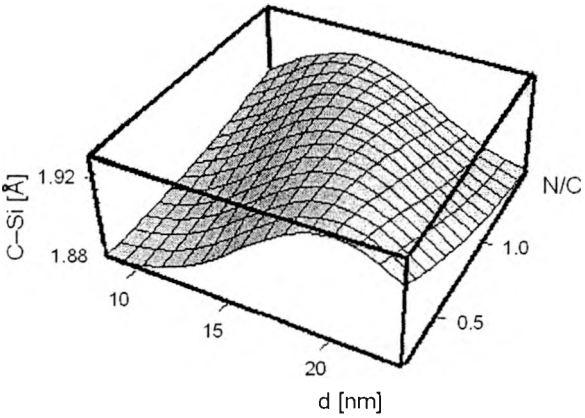

Fig. 1. Theoretical molecular dynamics geometry optimization of the C–Si bond distances *vs.* the film thickness *d* and the N/C ratio.

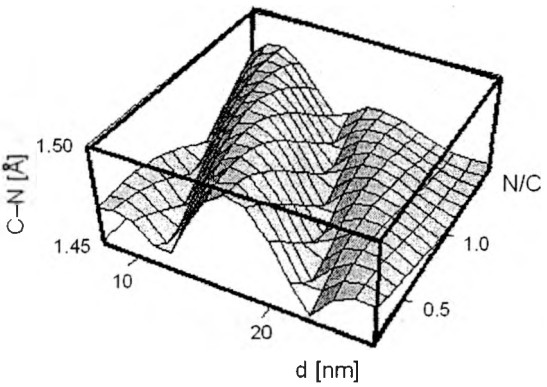

Fig. 2. Theoretical molecular dynamics geometry optimization of the C–N bond distances *vs.* the film thickness *d* and the N/C ratio.

1.45 Å for a film thickness range of 10–16 nm, the second one is at 1.465 Å within the thickness range of 18–24 nm. The appearance of two maxima suggests the existence of two possible minima of the local cluster total energy for the C–N bonds, in contrast to the C–Si bonds.

In order to check the reliability of our calculations, we have compared our theoretical results to those obtained from the EXAFS measurements. The examples presented in Fig. 3 (for C–Si) point to the similarity. The main differences are observed for the value of thickness at which the maxima appear. For lower N/C ratios the calculated peak is shifted towards higher thickness, while an increase in the N/C ratio decreases the shift, and for lager N/C ratio changes direction (*i.e.*, theoretical curves are shifted towards the lower thickness). The maximal shift can be observed for the N/C ratio of about 1.5. There are several possible causes for these differences: one is

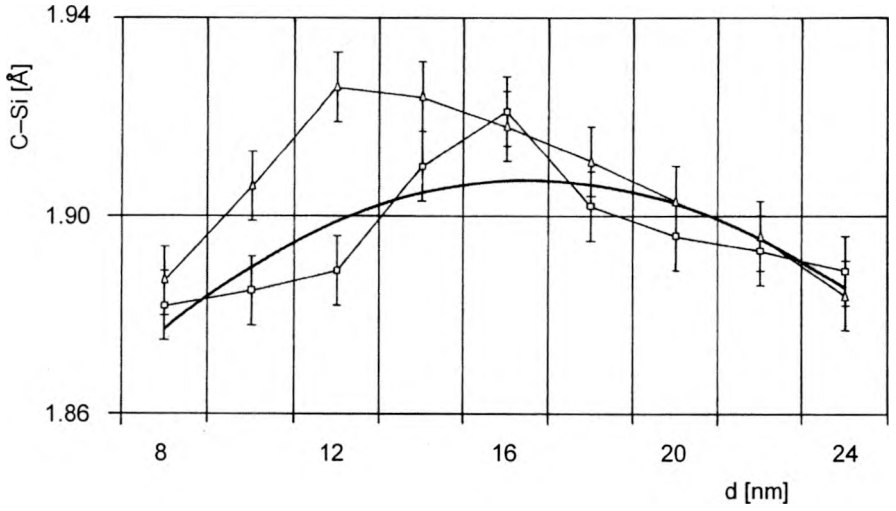

Fig. 3. C–Si bond distances as a function of the film thickness for the N/C ratios of: □ – 0.5, △ – 1.02. The solid line indicates the calculations without the electron–phonon interactions.

the non-homogeneity of the film stoichiometry distribution (up to 4.8%), another is the superposition of higher multiple interactions between the mesoscopic clusters.

5. Conclusions

A sufficient agreement between the experimental EXAFS data and theoretically simulated (by molecular dynamics and DFT) C–Si and C–N bond lengths indicates that the electron–phonon anharmonic interactions makes an important contribution to the observed phenomena. Theoretical simulations give a striking confirmation of the experimental C–Si and C–N distances for different N/C ratios.

Acknowledgments – Financial support from the State Committee for Scientific Research (KBN), Poland, through Pedagogical University, Częstochowa, Poland, grant (W.G., I.K.) is gratefully acknowledged.

References

[1] Semmache B., Lemiti M., Chanelier Ch., Dubois Ch., Sibai A., Canut B., Laugier A., Thin Solid Films **296** (1997), 32.
[2] Behrens K.-M., Klingenberg E.-D., Finster J., Meiwes-Breer K.-H., Surf. Sci. **402–404** (1998), 729.
[3] Habraken F.H.P.M., Appl. Surf. Sci. **30** (1987), 186.
[4] Kityk I.V., Kassiba A., Berdowski J., Plucinski K.J., Phys. Lett. A **265** (2000), 403.
[5] Plucinski K.J., Kityk I.V., Mefleh A., J. Non-Crystalline Solids **262** (2000), 143.
[6] Ceperley D.M. Alder B.J., Phys. Rev. Lett. **45** (1980), 566; Perdew B.J., Zunger A., Phys. Rev. B **23** (1981), 5048.
[7] Crozier E.D., Rehr J.J., Inggalls R., *X-ray Absorption*, [Ed.] D.C. Koningsberger, R. Prins, Willey, New York 1988.

[8] BECKE A.D., J. Chem. Phys. **98** (1994), 1372.
[9] SAHRAOUI B., KITYK I.V., NGUYEN PHU X., HUDHOMME P., GORGUES A., Phys. Rev. B **59** (1999), 9229.
[10] WASYLAK J., KUCHARSKI J., KITYK I.V., SAHRAOUI B., J. Appl. Phys. **85** (1999), 425.

Received May 13, 2002